Research article

Study of MI-BCI classification method based on the Riemannian transform of personalized EEG spatiotemporal features

Xiaotong Ding, Lei Yang* and Congsheng Li

China Academy of Information and Communications Technology, Beijing, China

* Correspondence: Email: yanglei@caict.ac.cn.

Abstract: Motor imagery (MI) is a traditional paradigm of brain-computer interface (BCI) and can assist users in creating direct connections between their brains and external equipment. The common spatial patterns algorithm is the most popular spatial filtering technique for collecting EEG signal features in MI-based BCI systems. Due to the defect that it only considers the spatial information of EEG signals and is susceptible to noise interference and other issues, its performance is diminished. In this study, we developed a Riemannian transform feature extraction method based on filter bank fusion with a combination of multiple time windows. First, we proposed the multi-time window data segmentation and recombination method by combining it with a filter group to create new data samples. This approach could capture individual differences due to the variation in time-frequency patterns across different participants, thereby improving the model's generalization performance. Second, Riemannian geometry was used for feature extraction from non-Euclidean structured EEG data. Then, considering the non-Gaussian distribution of EEG signals, the neighborhood component analysis (NCA) algorithm was chosen for feature selection. Finally, to meet real-time requirements and a low complexity, we employed a Support Vector Machine (SVM) as the classification algorithm. The proposed model achieved improved accuracy and robustness. In this study, we proposed an algorithm with superior performance on the BCI Competition IV dataset 2a, achieving an accuracy of 89%, a kappa value of 0.73 and an AUC of 0.9, demonstrating advanced capabilities. Furthermore, we analyzed data collected in our laboratory, and the proposed method achieved an accuracy of 77.4%, surpassing other comparative models. This method not only significantly improved the classification accuracy of motor imagery EEG signals but also bore significant implications for applications in the fields of brain-computer interfaces and neural engineering.

Keywords: Riemannian tangent space; motor imagery (MI); electroencephalogram (EEG); brain-

computer interface (BCI); filter banks; neighborhood component analysis

1.   Introduction

Using assistive technologies, the Brain Computer Interface (BCI) can establish communication and control between the human brain and computers or other electronic equipment. Electroencephalogram (EEG) can measure the scalp electrical activity generated by the brain and is non-invasive, low cost and has a high temporal resolution [1]. EEG signals commonly used in BCI systems include motor imagery (MI) [2], the P300 evoked potential [3] and the steady-state visual evoked potential (SSVEP) [4]. Among them, P300 and SSVEP are EEG signals based on the evoked patterns of external environmental stimuli. The difference is that MI is completely spontaneous. Therefore, the application prospect of MI is more extensive. BCI systems based on motor imagery EEG signals can help users establish direct channels between the brain and external devices for tasks such as manipulating two-armed robots, controlling drones and driving virtual cars [5].

When studying the brain activity during motor imagery, it is observed that the time-frequency patterns of oscillatory activity, which refer to the patterns of oscillatory activity across different time and frequency ranges, exhibit high variability across different participants [6]. Moreover, the event-related desynchronization (ERD) can vary significantly across individuals and be easily obscured during the data averaging process [7]. Therefore, accurate identification of the exact timing of MI occurrence is crucial for precise classification results. However, few studies have explored the impact of selecting different time windows for MI tasks on classification accuracy. In addition, the training set is relatively small due to the time-consuming and demanding nature of EEG data acquisition [7]. Therefore, data augmentation can assist the classification model in handling noise and outlier data, improving generalization capability and reducing overfitting. Based on this, we segmented the EEG signals into distinct time windows corresponding to the occurrence of MI tasks and subsequently recombined them. This strategy facilitated the capture of the specific time periods in which MI tasks transpired, effectively addressing the challenge of individual differences in MI-BCI. Furthermore, it broadened the training set, enabling the model to learn from an increased diversity of samples.

The EEG signals have low amplitude and low signal-to-noise ratio [5]. To extract EEG features, the most common solution is the application of the common spatial patterns (CSP) algorithm [8]. For binary MI task, the CSP algorithm maximizes the variance difference between the two types by using an optimal set of spatial filters to maximize the extraction of effective features. However, the performance of a conventional CSP algorithm depends mainly on the selection of a suitable operating band and time windows, which limits the classification accuracy [9,10]. Ang et al. [11] proposed the filter bank common spatial pattern (FBCSP), which extracted CSP features from each band after the EEG signal was bandpass filtered into multiple bands, and then, a feature selection algorithm was used to automatically select the recognition bands and the corresponding CSP features. However, the process had high computational costs. To overcome this problem, Thomas et al. [12] proposed the adaptive filter bank common spatial patterns (AFBCSP), which was based on the FBCSP. The AFBCSP selected the main band based on the time-frequency map of the Fisher ratio of the dichotomous motion imagery pattern. The results showed that the accuracy was similar to that of FBCSP, but the number of filters and the complexity of the computational method could be reduced.

Additionally, the covariance matrix constructed by the CSP method was susceptible to noise interference, which resulted in poor generalization performance of the CSP. This problem can be solved by Riemannian approaches [13] that use the knowledge of Riemannian geometry to directly manipulate the spatial EEG signal covariance matrix. Compared to Euclidean geometry, it introduces a more accurate approximation distance on smooth surfaces. Barachant et al. [14] improved the CSP algorithm based on the Riemannian mean. The Riemannian metric is better than the Euclidean metric in portraying the relevant information about class membership [13]. The CSP algorithm has a large bias in finding the mean point of the covariance matrix in the Euclidean space, and using the Riemannian centroid instead of the Euclidean mean point provides greater accuracy and better results. Nguyen et al. [15] used a multicore support vector machine to classify Riemannian features with an accuracy of 70.3%. Although the application of Riemannian geometry for EEG signal analysis led to several recent breakthroughs, a problem still needs to be solved. When a positive definite symmetric matrix is projected into the Euclidean space using the Riemann tangent space projection method, the dimensionality of the resulting vectors is frequently very high. Statistical bias might result from high-dimensional data. Thus, it is necessary to use the dimensionality reduction method to overcome the problem of excessive dimensionality. Principal component analysis (PCA) [16] and linear discriminant analysis (LDA) [17] are widely used for reducing the dimensionality of features. Notably, PCA and LDA may not be optimal for dimensionality reduction of data samples with non-Gaussian distributions. In contrast, the neighborhood component analysis (NCA) feature selection algorithm does not require specific assumptions about the distribution of the sample space. The NCA algorithm is more suitable for processing EEG signals.

Although the above methods achieved partly satisfactory results, they did not solve the problems of the individual variability in MI tasks and noise interference at the same time. In this study, we proposed an MI-BCI classification method based on the Riemannian transform with fused EEG spatiotemporal features. By segmenting the entire EEG data into time windows and subsequently combining them with spectral segmentation, we enhanced and reassembled the data. This process allowed us to extract features using Riemannian transformation and fuse them to ensure effective extraction of personalized ERD-related features. Our results indicated that the selection and combination of different time segments significantly impacted accuracy, and our proposed model effectively localized the ERD time periods, achieving accurate classification results. Then, after selecting features using the NCA feature selection algorithm, they were then fed into a SVM classifier to reduce model complexity and improve computational speed.

Notably, the method presented in this paper demonstrated an accuracy of 89% on the BCI Competition IV dataset 2a, surpassing existing state-of-the-art models, such as the lightweight multi-dimensional attention network, LMDA-Net, proposed by Miao et al. [18]. The LMDA-Net model combined two channel attention modules and depth attention modules, achieving an average accuracy of 78.8%. In comparison, our method significantly outperformed LMDA-Net in terms of classification accuracy.

Furthermore, in our laboratory dataset, our method achieved an accuracy of 77.4%, outperforming other comparative models. These findings highlighted the distinct superiority of our approach in addressing MI-BCI classification challenges, substantially enhancing the classification accuracy of motor imagery EEG signals, and providing robust support for research and applications in related fields.

2. Methods

A new structure was proposed in this study, and the framework of the method is shown in Figure 1. The method consisted of five stages, including temporal division, spectral division, Riemannian feature generation, NCA feature selection and support vector machine classification. The EEG data were initially segmented into predefined sub-time windows, followed by spectral segmentation within each sub-time window. The processed data were then combined to expand the training dataset and enhance the model's generalization performance. Subsequently, Riemannian features were computed for the data. To mitigate the high dimensionality of data after Riemannian feature extraction, feature selection methods were employed to reduce dimensionality, with the aim of reducing the model's complexity and minimizing computational costs. Finally, an optimal parameter combination for the four-class SVM classifier was determined through grid search and used to classify the EEG signals.
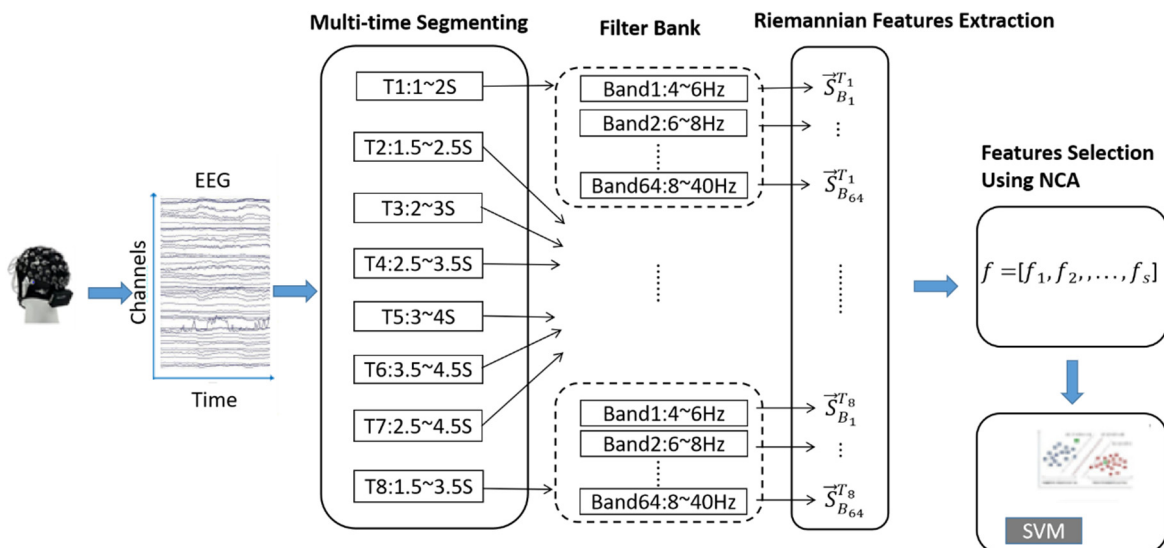

Figure 1. Flowchart of the proposed method.

2.1. Feature extraction

First, we calculated the covariance matrix of the EEG signal, which was processed by time segmentation and spectral segmentation. Next, the iterative gradient descent algorithm was used to calculate the Riemannian mean between n covariance matrices, and the Riemannian mean was used to calculate the Riemannian distance between multiple covariance matrices. Finally, the computed eigenmatrices were vectorized.

2.1.1. Multi-time segmentation

In the MI-based BCI system, subjects were asked to follow a cue to perform the corresponding MI task. Although the cueing time was known in the experimental paradigm, the reaction time of the brain to the MI task is usually unknown and may even be intermittent. In the MI paradigm, 0−1 s

after the cue is usually considered to be the imaginal preparation phase, while the time between 3.5 and 4 s is usually considered to be the imaginal end phase. Therefore, the selected EEG time window should be sufficient to cover the period when the brain was activated for MI, and should remove irrelevant data accordingly. Since the optimal time window varies between individuals, using a fixed single time window for data interception and pattern recognition might not yield the best classification performance.

For different MI tasks, the duration of ERD may vary. Typically, the duration of ERD ranges from several hundred milliseconds to a few seconds, depending on task type, individual differences and other factors. According to research [19], the ERD duration for imagining left and right hand movements is approximately 500 milliseconds. The ERD duration for imagining foot movements is usually around 1 second. The ERD duration for imagining tongue movements lasts for about 250 milliseconds. Therefore, the following method was employed to segment time windows, ensuring accurate capture of the ERD phenomenon. The original EEG signal was divided by time T1~T8. First, starting from the moment after cue, the EEG data were segmented with a length of 1 s, then time window was shifted with a step size of 0.5 s. Adhering to this pattern, time windows T1~T6 were segmented. Subsequently, based on the starting and ending times of the motor imagery tasks, T7~T8 were selected. Finally, each time window underwent frequency bands $(B_1 \sim B_{64})$ segmentation to extract specific frequency components. (We segmented the frequency band ranging from 4 to 40 Hz. We chose varying bandwidths (2, 4, 8, 16 and 32 Hz). During each frequency band segmentation, we used a sliding step size of 2 Hz.) The processed data were then combined to generate new samples encompassing multiple time periods and various frequency bands, thereby providing the model with more contextual information. This augmentation of feature richness improved classification accuracy.

2.1.2. Riemannian geometry

Let Set M be the G dimensional differentiable manifold, where $T_C M$ denotes the tangent space of M at $C\ (C \in M)$. Riemannian distance, also known as geodesic distance, is a very important metric that represents the distance of the shortest path between C and C' on a manifold M. The geodesic distance (δ_R) is equivalent to the length of its tangent vector [20] and can be expressed as follows:

$$\delta_R(C, C') = || \, log_C(C') \, ||_C = ||T'||_C \tag{1}$$

In Eq (1), $C, C' \in M$ and $T' \in T_C M$.

In this study, the knowledge of Riemannian geometry can be used to deal with spatial covariance matrices with symmetric positive definiteness. In the multi-classification case, the number of covariance matrices increases, and the mean value needs to be used as a metric. Let $\{D_i\}_{i=1}^n$ be a collection of n covariance matrices. Then, in the Riemannian manifold, the Riemannian mean of n covariance matrices [21] can be defined as the matrix that minimizes the sum of squares of the Riemannian distances.

$$\overline{D} = \vartheta(D_1, D_2, \ldots, D_n) = arg \min_D \sum_{i=1}^n \delta_R^2(D, D_i) \tag{2}$$

This mean does not have a closed-form solution. However, this problem can be solved using an iterative gradient descent algorithm [22] to find the Riemannian mean. The Riemannian mean can be

used to find a sum that minimizes the Riemannian distance of the covariance matrix with each trial. The Riemannian distance is defined as follows:

$$\delta_{\mathrm{R}}(C, C') = || \log(C^{-1}C') ||_{\mathrm{F}} = [\textstyle\sum_{i=1}^{N_c} \log^2 \lambda_i]^{\frac{1}{2}} \tag{3}$$

The EEG signals might be different for different people or even the same person at different times. The application of Riemannian distance and Riemannian mean can help solve the resulting degradation of classification accuracy. Barachant et al. [23] showed that for the same person, the EEG data at different times are assumed to have different Riemannian means, but the Riemannian distances for the same labeled data are approximately the same for the Riemannian means. Since the Riemannian distance and mean are robust to the noise in the Riemannian tangent space, projecting the covariance matrix into their corresponding tangent spaces and constructing the tangent vectors can make them effective as features of the classification algorithm.

2.2. Feature selection

In practical applications, Riemannian geometric methods often face the dimensional catastrophe problem. In this study, to solve the problems of non-smooth EEG signals and large individual differences, we used a multi-time window combination method, which increased the data dimension. Therefore, designing the dimensionality reduction algorithm is necessary. One purpose of feature selection is the suppression of irrelevant features to reduce the loss of information.

In this study, we used NCA [24] for Riemannian feature identification. This is a supervised learning method used for classifying a given metric in the data. No complicated matrix operation is required when using NCA for distance metrics or dimensionality reduction, and no specific assumptions about the distribution of the sample space are required. The NCA method minimizes the objective function by regularizing the ranking of the features and learning the feature weights. The metric of the objective function in the text is the average leave-one-out (LOO) classification loss on labeled training data.

The feature selection method of NCA is mainly based on the optimization of the nearest neighbor classification, which results in a weight vector w. According to the weight vector w, the weighted distance between two samples x_i and x_j is defined as:

$$d_w(x_i, x_j) = \textstyle\sum_{l=0}^{d} w_l^2 |x_{il} - x_{il}| \tag{4}$$

Here, w_l indicates the weight associated with the lth feature. The LOO technique maximizes the classification accuracy in the training set. When the error function is not continuous while calculating the error using the leave-one-out method, a differentiable softmax function is introduced as follows:

$$p_{ij} = \frac{exp(-||d_w(x_i,x_j)x_i - d_w(x_i,x_j)x_j||^2)}{\sum_{k \neq i} exp(-||d_w(x_i,x_j)x_i - d_w(x_i,x_j)x_k||^2)} \tag{5}$$

To define the function, we maximized the number of correctly classified points, i.e., the maximum likelihood of choosing comparable points as nearest neighbors accurately.

$$f(d_w) = \textstyle\sum_i \sum_{j \in C_i} p_{ij} = \sum_i p_i \tag{6}$$

Where f can be differentiated, and maximizing $f(d_w)$ is an unconstrained optimization problem, the conjugate gradient method can be used to iteratively solve the optimal value. The optimal solution of d_w can be obtained by continuous iterative optimization. Based on this, the obtained weight vector was used to rank the features and select the desired feature values as the classifier input.

2.3. Feature classification

SVM [25] is a typical classification algorithm for executing MI-BCI tasks. It finds an optimal hyperplane that maximizes the distance between two training data points. The support vector machine has flexible decision boundaries and a strong ability to generalize unknown information.

In this study, the One-Versus-Rest SVM was used for the four classification problems. Following this method, four SVMs were constructed for four categories of samples, and the unknown samples were placed in the category with the maximum classification function value. In addition, the optimal SVM parameters were determined by using the grid search [26]. By traversing a given parameter space, a model was trained for each parameter combination and evaluated using cross-validation to assess model performance. The parameter combination that achieved the optimal model performance was selected as the optimal parameters for the SVM model.

3. Materials

3.1. Public dataset

The BCI competition IV dataset 2a contains EEG data from nine healthy subjects who were required to perform four motor imagery tasks, which included imagined movements of the left hand, right hand, feet and tongue. Each participant had to complete two phases of data acquisition, including a training set data acquisition and a test set acquisition. In total, 25 measurement channels were used to record the dataset, including 22 EEG channels and three monopolar electrooccular (EOG) channels. The dataset was uploaded to https://www.bbci.de/competition/iv/#datasets.

3.2. Experimentally collected dataset

The data were collected from healthy participants who had no experience with MI-based BCI (n = 7 males, 22−26 years old). All subjects signed an informed consent form before the experiment and were designated as sub-001 to sub-007. The study was approved by the Medical Ethics Committee of Chinese PLA General Hospital.

The EEG data were acquired using a 64-channel gel electrode cap (according to the standard 10/20 system) and a Neuroscan SynAmps2 amplifier (Neuroscan, Inc.). The sampling frequency was 250 Hz. The EEG measurements were made using the left mastoid fiducial. During the experiment, the electrode impedance was kept below 10 kΩ. The bandpass filtering range of the system was 0.5−100 Hz.

The subject wearing the electrode cap sat on a chair with both hands naturally resting on the thighs and both eyes 1 m away from the screen (see Figure 2). As shown in Figure 2, at the beginning of each trial, a short "ding" sound was emitted, and a cross-arrow appeared at the center of the display. The cross-arrow was presented for 2 seconds to prompt that the experiment was about to begin. Subsequently, the target arrow representing the motor imagery task was displayed on the screen for 4

seconds. During this time, the subjects were asked to imagine the movements ("left hand", "right hand", "feet" and "tongue") instead of visualizing the picture that corresponded to them. The terms "left hand" and "right hand" represented lifting the respective left and right hands, "feet" represented lifting both feet and "tongue" represented rolling up the tongue. The researchers asked the participants not to make any movements while imagining. At the end of the imagery task, the screen turned black for 2 s and the 8-s trial ended.
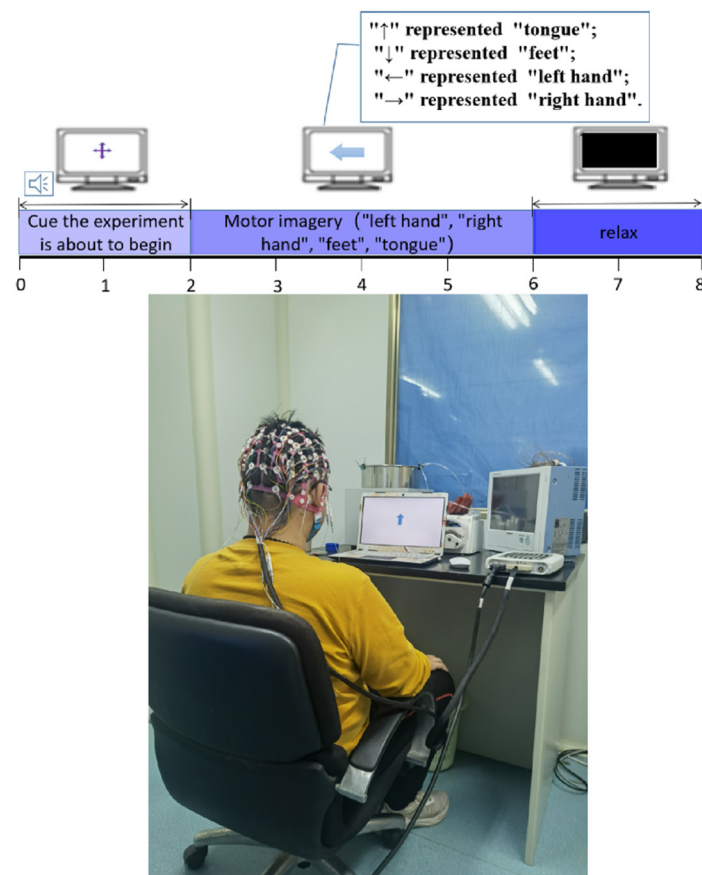

Figure 2. Experimental procedure for each participant.

The experiment consisted of six sessions. Each session consisted of 12 trials of each of the four motor imagery tasks. To prevent mutual influence between the former and latter tasks, they appeared randomly. There was a 5 to 10 min break between sessions. Some channel data were excluded during the data processing stage, and 22 channels relevant to the motor imagery task were selected for processing.

4. Results

4.1. Experimental results

The performance of the method proposed in this study was compared to other representative methods by conducting extensive experiments. We chose CSP as the baseline model, and compared it with FBCSP, AFBCSP, CNN-SAE and the proposed method in this study.

1) CSP: The feature extraction of the EEG signal from 0−4 s was performed in the range of 8–40 Hz using the CSP technique.

2) FBCSP [27]: CSP features were extracted from EEG data, which were based on multiple frequency bands throughout the time window. Based on this, the optimal feature selection method was used to automatically select the corresponding filter banks and CSP features.

3) AFBCSP: The discriminative frequency components of a particular subject were first selected using the time-frequency map of fisher ratios of motion picture patterns. Then, the subject-specific bandpass filter was selected adaptively based on the information from Fisher's ratio time-frequency map. The features were extracted only from the selected frequency components.

4) CNN-SAE [28]: By conditioning the filters of the CNN convolutional layer, the features of the input EEG signal were retrieved. Then, a deep SAE network used these attributes to classify the data.

The filtered EEG data were classified using an SVM classifier after applying the relevant methods described above to extract features. Based on the results of the grid search, a linear function was used as the kernel with the optimal classification parameters. The classification effectiveness of the two datasets was evaluated using 10-fold cross-validation.

The classification accuracy for all subjects in both datasets was summarized in Tables 1 and 2. The classification accuracy refers to the proportion of samples that are correctly classified by the classifier among all the testing samples. It is calculated as the number of correct predictions divided by the total number of predictions. The proposed method achieved the highest classification accuracy in both datasets. Among them, the average accuracy for the nine subjects in the BCI competition IV dataset 2a was 68.8% (CSP), 62.5% (FBCSP), 75.4% (CNN-SAE), 70.6% (AFBCSP) and 89.00% (the proposed method). The kappa values [29] of each method were also calculated for all subjects. The kappa value of the proposed method in this study was 0.73 (Table 1), and its classification performance was significantly better than that of the other methods.

Table 1. The classification accuracy of different methods for nine subjects in the BCI competition IV dataset 2a.

Subject	Method				
	CSP+SVM	FBCSP+SVM	AFBCSP+SVM	CNN-SAE	Proposed method
sub-001	0.810	0.701	0.851	0.861	**0.925**
sub-002	0.678	0.609	0.598	0.678	**0.901**
sub-003	0.816	0.83	0.805	**0.90**	0.899
sub-004	0.494	0.598	0.540	0.64	**0.899**
sub-005	0.598	0.71	0.747	0.733	**0.926**
sub-006	0.322	0.436	0.402	0.502	**0.831**
sub-007	0.874	0.862	0.874	0.914	**0.941**
sub-008	0.851	0.805	0.86	**0.897**	0.894
sub-009	0.747	0.780	0.644	0.665	**0.798**
mean ± std	0.688 ± 0.175	0.625 ± 0.137	0.706 ± 0.161	0.754 ± 0.137	**0.890** ± 0.044
kappa	0.52	0.57	0.63	0.60	**0.73**

Table 2. The classification accuracy of different methods for the seven subjects in the experimentally collected dataset.

Subject	Method				
	CSP+SVM	FBCSP+SVM	AFBCSP+SVM	CNN-SAE	Proposed method
sub-001	0.344	0.698	0.583	0.688	**0.750**
sub-002	0.411	0.555	0.543	0.572	**0.761**
sub-003	0.477	0.805	0.796	**0.849**	0.769
sub-004	0.360	0.538	0.556	0.551	**0.776**
sub-005	0.443	0.444	0.45	0.625	**0.751**
sub-006	0.443	0.403	0.574	0.764	**0.80**
sub-007	0.442	0.774	0.783	0.792	**0.812**
mean ± std	0.417 ± 0.045	0.602 ± 0.147	0.612 ± 0.119	0.692 ± 0.105	**0.774** ± 0.022

To provide an intuitive comparison of the performance of each model in public dataset, we employed Receiver Operating Characteristic (ROC) curves as the evaluation metric. Based on the previously discussed results, we selected the following models for comparison: FBCSP+SVM, AFBCSP+SVM, CNN-SAE and the proposed method.

As shown in Figure 3, the ROC curve of our proposed method was situated closest to the upper left corner, signifying a high true positive rate and a low false positive rate. Conversely, the ROC curves of the other three models exhibited a slight deviation from the optimal position. These observations suggested that the proposed method outperformed the other models in terms of classification accuracy.
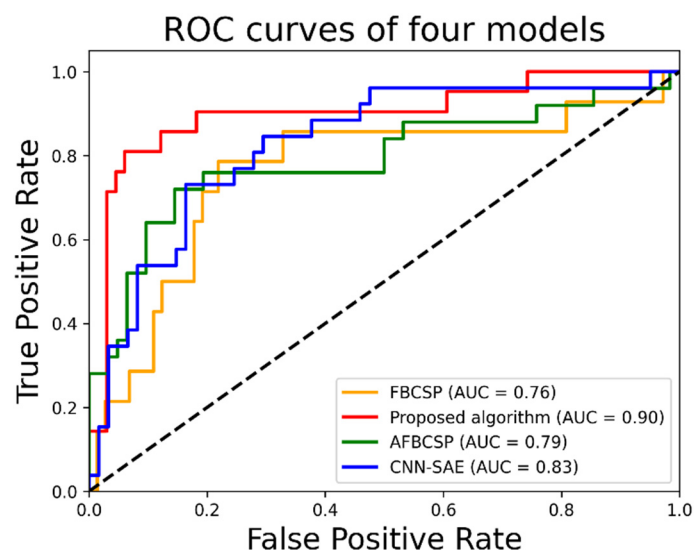

Figure 3. Comparative study of ROC curves for four models.

To further support our findings, we computed the Area Under Curve (AUC) values for each model. The AUC value represents the area beneath the ROC curve and serves as a quantitative measure of a model's performance. An AUC value approaching 1 indicates superior performance.

Our calculations showed that the proposed method achieved the highest AUC value (AUC = 0.90).

In contrast, FBCSP+SVM (AUC = 0.76), AFBCSP+SVM (AUC = 0.79) and CNN-SAE (AUC = 0.83) demonstrated lower AUC values. These results corroborated the conclusions drawn from the ROC curve observations, further confirming the superior performance of the proposed method in MI tasks. With its high accuracy, the proposed method provided robust support for research and applications in this domain.

4.2. Comparison of classification effects with different time windows

The classification accuracy obtained by combining the EEG data with different time windows for all subjects in public dataset is shown in Figure 4. We found that the classification of the combined pattern of time windows was the best among the participants sub-003, sub-007 and sub-009. The sub-time windows T_1, T_3 and T_5 of sub-003 and sub-009 had higher classification accuracy. The sub-time windows T_1, T_2 and T_3 of sub-007 had higher classification accuracy. This illustrated that different subjects had different response times for the MI task. Additionally, as shown in Figure 4, the accuracy of using a single time window for classification was significantly lower than that of using multi-time window combination algorithm for classification. It also indicated that the proposed multi-time window combination algorithm could reduce the risk of misclassification due to improper time window selection.
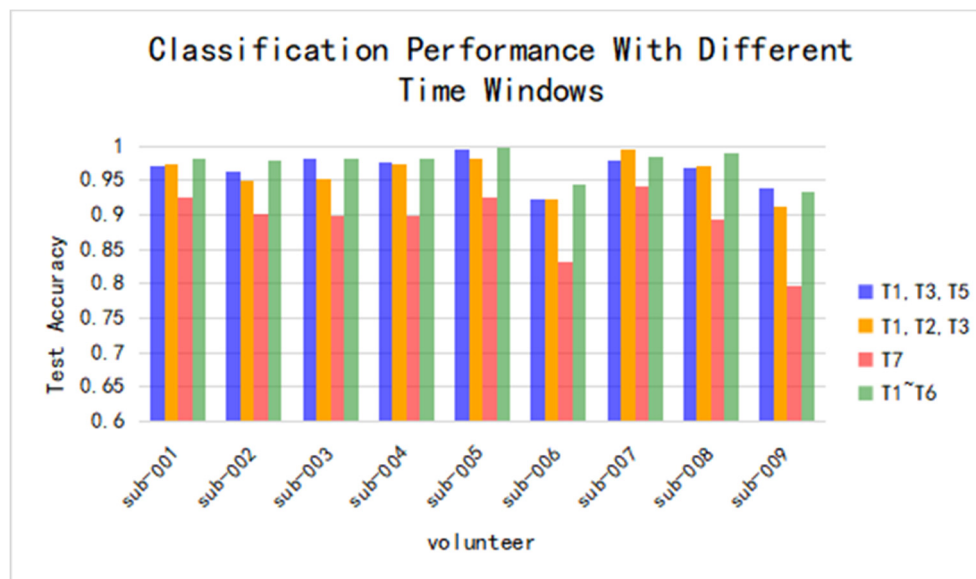

Figure 4. Effect of choosing different time windows on classification accuracy.

4.3. Comparative analysis of feature distributions

To facilitate the comparison of feature distribution, the dataset was divided into two categories, and only left-handed and right-handed tasks were processed. To illustrate the results, the data of sub-002 in public dataset, who showed average performance, were selected for the analysis. The distribution of the two features obtained in Riemannian space and Euclidean space is shown in Figure 5. Figure 5(b) indicated that the performance of extracting EEG signal feature distributions in the Euclidean space was poor. In contrast, Figure 5(a) showed that the algorithm based on the Riemannian

transform provided a more easily separable distribution of features. This conclusion was consistent with the findings of the discussion of the method in Section II and the classification performance of Tables 1 and 2.
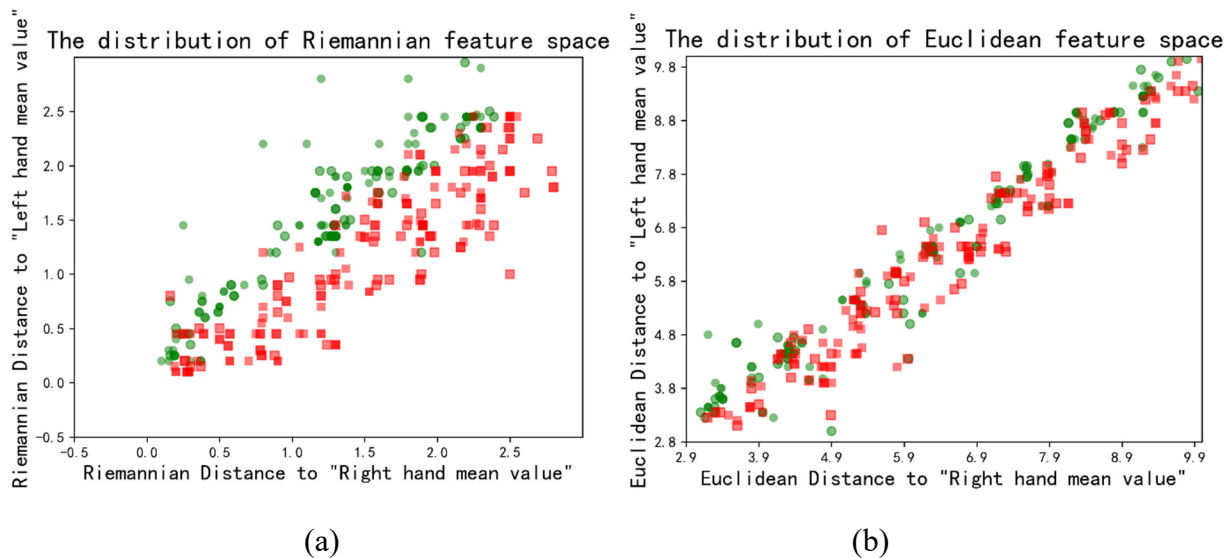

(a)   (b)

Figure 5. (a) The distribution of Riemannian distances relative to the Riemannian mean for the right-hand and left-hand covariance matrices. (b) The distribution of Euclidean distances relative to Euclidean means for the right-hand and left-hand covariance matrices. (The red dots represented the distribution of features from the right hand, and the green dots represented the distribution of features from the left hand.)

4.4. Computational efficiency

The computational efficiency of several of the above-mentioned comparison algorithms was analyzed by using the example of sub-002 in public dataset. The testing time required to perform one experiment using python 3.9 on a PC is shown in Table 3. This PC is equipped with an i5-9600K 3.7GHz CPU and 16GB RAM, meeting the computing requirements for our experiments. The results showed that the method proposed in the study was not the fastest but was able to achieve real-time processing (computation time was less than the experimental time) [30]. Most of the time was spent training the model. However, testing occurred almost immediately, requiring only about 738 ms. Thus, the method could effectively improve the classification accuracy of BCI without affecting the computational speed of BCI.

Table 3. Comparison of the time spent by different methods to perform calculations.

Subject			Method		
	CSP+SVM	FBCSP+SVM	AFBCSP+SVM	CNN-SAE	Proposed method
Computation time (ms)	508	708	600	400	738

4.5. Ablation study

We performed ablation analyses on the BCI competition IV dataset 2a to further investigate the effectiveness of the multi-time window combination module and NCA module in the proposed method. We removed the multi-time window combination module and the NCA module in turn and compared them with the proposed method. As shown in Figure 6, both the multi-time window combination and NCA modules had contributed to the improvement of the classification accuracy. Moreover, it could be clearly observed that the classification accuracy of features extracted from fixed time windows (1−4 s) exhibited substantial individual variability and instability. In contrast, the proposed multi-time window combination model significantly enhanced the generalization performance of MI classification tasks.
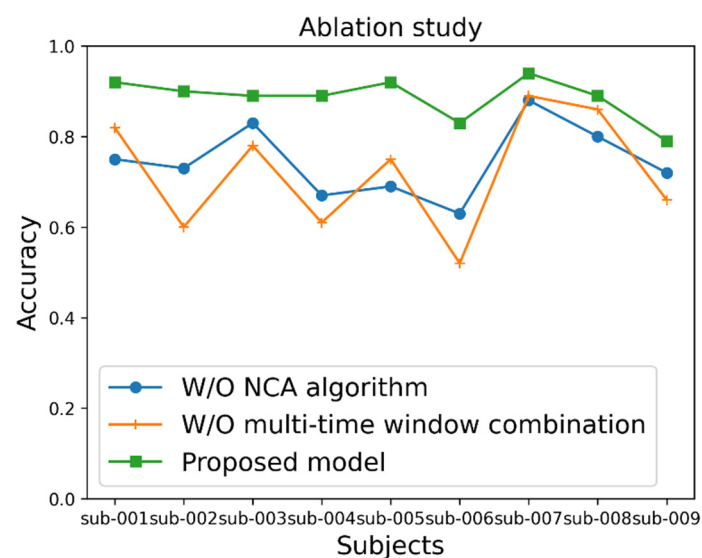

Figure 6. Comparison of accuracy in the proposed model under different ablative conditions. W/O NCA algorithm represented the proposed model without NCA algorithm module; W/O multi-time window combination represented the proposed model without multi-time window combination module.

5. Discussion

In MI-BCI, CSP is the most common spatial feature extraction technique. However, the algorithm is highly sensitive to noise and has weak generalization performance. To enhance the generalization performance of CSP, many studies have investigated ways to improve the CSP algorithm. In this study, the idea of combining multiple filters in the FBCSP algorithm was used to extract the EEG data of the α-band (8−12 Hz) and the β-band (12−30 Hz) [31]. Then, the sub-band filter bank was utilized to further divide the EEG data segmented by time windows. Previous studies analyzed only the frequency domain and did not focus on the response speed of the subject in the MI task. The response latencies of the MI tasks were different (Figure 4). In BCI experiments, variance can be due to time variability, session-to-session variability or subject-to-subject variability. Therefore, variance probably is an important source of error. Combining time window may be a way of solving this variability problem,

which may explain its success. In this study, we divided the MI cycle into different sub-time windows to combine multiple time windows. Using this strategy, we solved the problem of finding the optimal instant for classification.

Since the Riemannian distance and mean were robust to the noise in the Riemannian tangent space, the covariance matrix could be operated to improve the distribution of the features in the Euclidean space, making them more effective as features of the classification algorithm (Figure 5).

Feature selection is the key to MI classification. When selecting features that are relevant to the completion of the classification, irrelevant or less important features that have a low impact on the classification goal need to be discarded. Features that are irrelevant or not fully relevant can have a detrimental effect on the execution of the model. The commonly used PCA feature reduction method was compared to the NCA feature selection method used in this study. As shown in Figure 7, the scatter plot of the selected feature distribution showed that the features selected by the NCA had better separability.
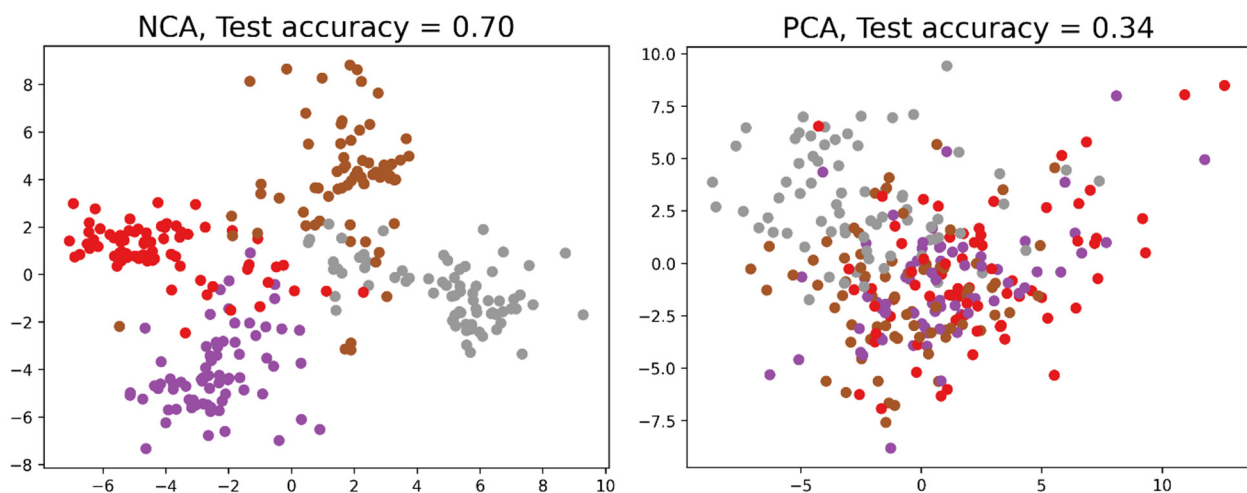

Figure 7. Comparison of the PCA feature reduction method and the NCA feature selection method. (The red dots represented the 'right hand', the purple dots represented the 'left hand', the gray dots represented the 'tongue', and the brown dots represented the 'feet'.)

We used machine learning instead of deep learning because we verified via experiments that the method in this study could achieve similar or higher accuracy while the complexity of using machine learning was lower, and the calculation cost was lesser. To achieve high performance, deep learning requires very large datasets. For MI-BCI, such a large dataset is not readily available. For smaller datasets, machine learning often outperforms deep learning. Also, machine learning is more interpretable.

Besides, we conducted a quantitative comparison between our model and the existing state-of-the art model LMDA-Net model. LMDA-Net incorporated two novel attention modules designed specifically for EEG signals, the channel attention module and the depth attention module, LMDA-Net was able to effectively integrate features from multiple dimensions, resulting in improved classification performance across various BCI tasks. On the BCI Competition IV dataset 2a, LMDA-Net achieved an average accuracy of 78.8%, a kappa value of 0.71 and an AUC value of 0.74. However, upon evaluation, our model achieved an average accuracy of 89%, a kappa value of 0.73 and an AUC

value of 0.9. Compared to the LMDA-Net model, our model exhibited significant improvements in all performance metrics, indicating that our model possessed higher accuracy and robustness in motor imagery classification tasks. The differences in performance might be attributed to the effective capture of ERD time periods in our model and the advantages of using Riemannian transformation for feature extraction. Moreover, our model reduced complexity and improved computational speed through the use of the NCA feature selection algorithm and an SVM classifier. In contrast, while LMDA-Net achieved some success in integrating multi-dimensional features, it still lagged behind in terms of classification accuracy.

Although the method outperformed other methods regarding performance, further refinements are needed in the following area. The multi-temporal window combination model proposed in this study can solve the problem of variability for classification, but the training time needs to be extended as the choice of time windows increases. Further study is needed to improve this aspect. For instance, implementing parallel computing can effectively reduce computation time by decomposing tasks into multiple sub-tasks and executing them concurrently. Taking advantage of multi-core processors or GPU acceleration for parallel processing can significantly speed up calculations, thus mitigating the extended training times associated with our current approach. Moreover, in future research, we could consider combining Multiple Graph Cooperative Learning Neural Networks (MGLNN) proposed by Jiang et al. [32]. Applying MGLNN to MI-BCI classification tasks can extract valuable information regarding MI by simultaneously processing multiple graph structures based on time windows, frequency bands, or brain regions. By introducing this advanced technique, we expect to further improve the performance of MI-BCI classification.

6. Conclusions

In this study, we developed a MI-BCI classification method based on Riemannian geometry, which classified the fused EEG spatiotemporal frequency features. Our approach employed the combination of multiple sub-time windows to tackle the challenge of individual variability in EEG classification. Subsequently, we employed Riemannian geometry to extract features, overcoming the problem of low signal-to-noise ratio and improving the discriminability of features. Finally, we applied the NCA feature selection algorithm, which was more suitable for processing EEG signals, to reduce data dimensionality while minimizing model complexity, so that the processed features could be input into the SVM classifier for faster computation. This method enhanced the accuracy and stability of the MI-BCI system. In conclusion, the proposed method significantly enhanced the classification performance of EEG signals, laying a solid foundation for further research and practical applications in the BCI field.

Acknowledgments

Conflict of interest

All authors declare no conflicts of interest in this paper.

References

1. W. G. Zhang, L. Lu, A. N. Belkacem, J. X. Zhang, P. H. Li, J. Liang, et al., Classification of EEG signals based on GA-ELM optimization algorithm, in *Human Brain and Artificial Intelligence* (eds. X. M. Ying), HBAI, **1692** (2022), 3−14. https://doi.org/10.1007/978-981-19-8222-4_1

2. R. Sharma, M. Kim, A. Gupta, Motor imagery classification in brain-machine interface with machine learning algorithms: classical approach to multi-layer perceptron model, *Biomed. Signal Process. Control*, **71** (2022), 103101. https://doi.org/10.1016/j.bspc.2021.103101

3. W. S. Pritchard, Psychophysiology of P300, *Psychol. Bull.*, **89** (1981), 506−540. https://doi.org/10.1037/0033-2909.89.3.506

4. A. M. Norcia, L. G. Appelbaum, J. M. Ales, B. R. Cottereau, B. Rossion, The steady-state visual evoked potential in vision research: a review, *J. Vision*, **15** (2015), 4. https://doi.org/10.1167/15.6.4

5. G. Pfurtscheller, G. R. Muller-Putz, R. Scherer, C. Neuper, Rehabilitation with brain-computer interface systems, *Computer*, **41** (2008), 58−65. https://doi.org/10.1109/MC.2008.432

6. C. Neuper, R. Scherer, M. Reiner, G. Pfurtscheller, Imagery of motor actions: differential effects of kinesthetic and visual-motor mode of imagery in single-trial EEG, *Cognit. Brain Res.*, **25** (2005), 668−677. https://doi.org/10.1016/j.cogbrainres.2005.08.014

7. F. Lotte, L. Bougrain, A. Cichocki, M. Clerc, M. Congedo, A. Rakotomamonjy, et al., A review of classification algorithms for EEG-based brain-computer interfaces: a 10-year update, *J. Neural Eng.*, **15** (2018), 031005. https://doi.org/10.1088/1741-2552/aab2f2

8. U. Talukdar, S. M. Hazarika, J. Q. Gan, Adaptive feature extraction in EEG-based motor imagery BCI: tracking mental fatigue, *J. Neural Eng.*, **17** (2020). https://doi.org/10.1088/1741-2552/ab53f1

9. F. Lotte, C. T. Guan, Regularizing common spatial patterns to improve BCI designs: unified theory and new algorithms, *IEEE Trans. Biomed. Eng.*, **58** (2011), 355−362. https://doi.org/10.1109/TBME.2010.2082539

10. J. Jiang, C. H. Wang, J. H. Wu, W. Qin, M. P. Xu, E. W. Yin, Temporal combination pattern optimization based on feature selection method for motor imagery BCIs, *Front. Hum. Neurosci.*, **14** (2020), 231. https://doi.org/10.3389/fnhum.2020.00231

11. K. K. Ang, Z. Y. Chin, H. H. Zhang, C. T. Guan, Filter bank common spatial pattern (FBCSP) in brain-computer interface, in *IEEE International Joint Conference on Neural Networks*, 2008. https://doi.org/10.1109/IJCNN.2008.4634130

12. K. P. Thomas, C. T. Guan, L. C. Tong, V. A. Prasad, An adaptive filter bank for motor imagery based brain computer interface, in *International Conference of the IEEE Engineering in Medicine & Biology Society*, Vancouver, BC, Canada, 2008. https://doi.org/10.1109/IEMBS.2008.4649353

13. A. Barachant, S. Bonnet, M. Congedo, C. Jutten, Multiclass brain–computer interface classification by Riemannian geometry, *IEEE Trans. Biomed. Eng.*, **59** (2012), 920−928. https://doi.org/10.1109/TBME.2011.2172210

14. A. Barachant, S. Bonnet, M. Congedo, C. Jutten, Common spatial pattem revisited by Riemannian geometry, in *Proceedings of the 2010 IEEE International Workshop on Multimedi a Signal Processing*, (2010), 472−476. https://doi.org/10.1109/MMSP.2010.5662067

15. C. H. Nguyen, P. Artemiadis, EEG feature descriptors and discriminant analysis under Riemannian manifold perspective, *Neurocomputing*, **275** (2018). https://doi.org/10.1016/j.neucom.2017.10.013

16. H. Abdi, L. J. Williams, Principal component analysis, *WIREs Comput. Stat.*, **2** (2010), 433−459. https://doi.org/10.1002/wics.101

17. J. Shao, Y. Z. Wang, X. W. Deng, S. J. Wang, Sparse linear discriminant analysis by thresholding for high dimensional data, *Ann. Stat.*, **39** (2011), 1241−1265. https://doi.org/10.1214/10-AOS870

18. Z. Q. Miao, X. Zhang, M. R. Zhao, D. Ming, LMDA-Net: a lightweight multi-dimensional attention network for general EEG-based brain-computer interface paradigms and interpretability, preprint, arXiv:2303.16407.

19. C. Neuper, G. Pfurtscheller, Evidence for distinct beta resonance frequencies in human EEG related to specific sensorimotor cortical areas, *Clin. Neurophysiol.*, **112** (2001), 2084−2097. https://doi.org/10.1016/S1388-2457(01)00661-7

20. O. Tuzel, F. Porikli, P. Meer, Pedestrian detection via classification on Riemannian manifolds, *IEEE Trans. Pattern Anal. Mach. Intell.*, **30** (2008), 1713−1727. https://doi.org/10.1109/TPAMI.2008.75

21. M. Moakher, A differential geometric approach to the geometric mean of symmetric positive-definite matrices, *SIAM J. Matrix Anal. Appl.*, **26** (2005), 735−747. https://doi.org/10.1137/S0895479803436937

22. P. T. Fletcher, S. Joshi, Principal geodesic analysis on symmetric spaces: statistics of diffusion tensors, in *Computer Vision and Mathematical Methods in Medical and Biomedical Image Analysis*, (2004), 87−98. https://doi.org/10.1007/978-3-540-27816-0_8

23. A. Barachant, S. Bonnet, M. Congedo, C. Jutten, Classification of covariance matrices using a Riemannian-based kernel for BCI applications, *Neurocomputing*, **112** (2013), 172−178. https://doi.org/10.1016/j.neucom.2012.12.039

24. J. Goldberger, S. T. Roweis, G. E. Hinton, R. R. Salakhutdinov, Neighbourhood components analysis, in *Proceedings of the 17th International Conference on Neural Information Processing Systems*, Vancouver British Columbia Canada, (2004), 513−520. Available from: https://proceedings.neurips.cc/paper/2004/file/42fe880812925e520249e808937738d2-Paper.pdf.

25. H. Y. Sun, Y. Xiang, Y. R. Sun, H. P. Zhu, J. H. Zeng, On-line EEG classification for brain-computer interface based on CSP and SVM, in *2010 3rd International Congress on Image and Signal Processing*, (2010), 4105−4108. https://doi.org/10.1109/CISP.2010.5648081

26. I. Syarif, A. Prugel-Bennett, G. Wills, SVM parameter optimization using grid search and genetic algorithm to improve classification performance, *TELKOMNIKA*, **14** (2016), 1502−1509. http://doi.org/10.12928/telkomnika.v14i4.3956

27. K. K. Ang, Z. Y. Chin, C. C. Wang, C. T. Guan, H. H. Zhang, Filter bank common spatial pattern algorithm on BCI competition IV datasets 2a and 2b, *Front. Neurosci.*, **6** (2012), 39. https://doi.org/10.3389/fnins.2012.00039

28. Y. R. Tabar, U. Halici, A novel deep learning approach for classification of EEG motor imagery signals, *J. Neural Eng.*, **14** (2017), 016003. https://doi.org/10.1088/1741-2560/14/1/016003

29. J. Carletta, Assessing agreement on classification tasks: the Kappa statistic, *Comput. Ling.*, **22** (1996), 249−254. Available from: https://aclanthology.org/J96-2004.pdf.

30. Y. Y. Miao, J. Jin, I. Daly, C. Zuo, X. Y. Wang, A. Cichocki, et al., Learning common time-frequency-spatial patterns for motor imagery classification, *IEEE Trans. Neural Syst. Rehabil. Eng.*, **29** (2021), 699−707. https://doi.org/0.1109/TNSRE.2021.3071140

31. K. Raj, A. Singh, A. Mandal, T. Kumar, A. M. Roy, Understanding EEG signals for subject-wise Definition of Armoni Activities, preprint, arXiv:2301.00948.

32. B. Jiang, S. Chen, B. B. Wang, B. Luo, MGLNN: semi-supervised learning via multiple graph cooperative learning neural networks, *Neural Networks*, **153** (2022), 204−214. https://doi.org/10.1016/j.neunet.2022.05.024